Wind and Structures, Vol. 10, No. 3 (2007) 215-232
DOI: http://dx.doi.org/10.12989/was.2007.10.3.215

A study of wind effect on damping and frequency of a long span cable-stayed bridge from rational function approximation of self-excited forces

Shambhu Sharan Mishra†

Department of Civil Engineering, NERIST, Nirjuli, Arunachal Pradsh-791109, India

Krishen Kumar‡ and Prem Krishna‡†

Department of Civil Engineering, Indian Institute of Technology, Roorkee-247667, India

(Received May 29, 2006, Accepted February 22, 2007)

Abstract. This paper presents an aeroelastic analysis procedure to highlight the influence of wind velocity on the structural damping and frequency of a long span cable-stayed bridge. Frequency dependent self-excited forces in terms of flutter derivatives are expressed as continuous functions using rational function approximation technique. The aeroelastically modified structural equation of motion is expressed in terms of frequency independent modal state-space parameters. The modal logarithmic dampings and frequencies corresponding to a particular wind speed are then determined from the eigen solution of the state matrix.

Keywords: cable stayed bridge; bridge aerodynamics; aeroelastic response; frequency; damping; rational function approximation.

1. Introduction

Long span cable-supported bridges are susceptible to wind induced oscillations and therefore, the aerodynamic performance of such bridges has been a major concern to designers. The aerodynamic behaviour of complex three dimensional cable-stayed bridges is vexed. These bridges are inherently flexible and as a consequence they have low values of natural frequency and damping. The natural frequencies are often contiguous and, the ratio of the fundamental torsional to the vertical mode frequency is low which increases the prospect of coupling of modes resulting in flutter under strong winds (Jain, *et al*. 1996a, b, Katsuchi, *et al*. 1998, Chen, *et al*. 2000b). Flutter is a phenomenon due to self-excited forces in which aerodynamic forces, elasticity and inertia of the bridge motion interact with each other. The self-excited forces depend on the flutter derivatives which are determined experimentally. Some investigators, notably Scanlan, *et al*. (1974), Scanlan (1993), Chen and Kareem

† Professor, Corresponding Author, E-mail: chadyaneha_sunny@yahoo.co.in
‡ Former Professor
‡† Visiting Professor, Email: iswe@iitr.ernet.in

(2002) and Caracoglia and Jones (2003) have highlighted the use of indicial or impulse response functions to express the aerodynamic forces in the explicit time domain. However, the techniques to determine these functions from the wind tunnel tests are not well established. Also, the experimental set up required is very complicated. The values of indicial functions obtained are even more questionable for bluff bridge deck sections (Caracoglia and Jones 2003). On the contrary, the techniques to determine the flutter derivatives are well established, and as a convention the self-excited forces are expressed in terms of the flutter derivatives which are frequency dependent. Thus, the self-excited forces incorporate the frequency dependent characteristics of unsteady aerodynamic forces. The flutter derivatives are determined experimentally through a system identification technique in frequency or time domain, and are available corresponding to discrete values of reduced velocity. The experiment is conducted on an elastically supported and geometrically scaled representative section model of the bridge deck oscillating under a two dimensional wind flow in a wind tunnel. The oscillations imparted to the section model in the lift, drag and pitching directions may be free, forced or wind induced (Hjorth-Hansen 1992, Mishra, *et al*. 2006). The self-excited forces modify the stiffness (hence frequency), damping and mode shape characteristics of the bridge under increasing wind.

The flow around the bridge deck section in particular is quite unsteady. Therefore, proper modeling of the aerodynamic forces incorporating all the unsteady aerodynamic characteristics is essential for an accurate evaluation of the bridge response. The frequency dependent unsteady aerodynamic forces have traditionally been utilized in the frequency domain aeroelastic analysis of long span cable-stayed bridges (Jain, *et al*. 1996a, b, Katsuchi, *et al*. 1998, Scanlan 1978, Lin and Yang 1983, Scanlan and Jones 1990, Jones and Scanlan 1991, Tanaka, *et al*. 1992, Jones and Scanlan 2001). However, the frequency domain analysis is suited only to linear aerodynamics. On the contrary, the time domain analysis approach can make it possible to incorporate all the structural and aerodynamic nonlinearities of the system.

In this paper, an example long span cable-stayed bridge has been taken for the study of the influence of aeroelastic forces due to increasing wind on frequency and damping of the system. A nonlinear static analysis of the bridge was carried out by considering the nonlinear stiffness formulation of the bridge structure. This analysis is not presented here for brevity and, can be found in Mishra (2005). The deformed state stiffness matrix is taken for the subsequent dynamic and aeroelastic analyses. A nonlinear aeroelastic force model with time domain approach (Boonyapinyo, *et al*. 1999, Chen, *et al*. 2000a, b, Chen and Kareem 2002) is used to study the influence of increasing wind velocities on the frequency and damping characteristics of the bridge. Since flutter derivatives are known only at discrete values of the reduced frequencies, they are expressed as appropriate continuous functions of the reduced frequency. The approach uses rational function approximation of experimentally determined flutter derivatives. This enables the unsteady self-excited forces to be expressed in the Laplace frequency domain. The modal equation of motion, when transformed back to time domain, yields frequency independent state-space form of equation. The unsymmetric state matrix thus obtained yields complex eigenvalues from which the frequency and logarithmic damping values are determined. The method avoids iterative calculation and is computationally efficient. In the sections that follow, the methodology outlined is used to present the results of the investigation.

2. Aeroelastic force model

The aeroelastic force vector $\boldsymbol{f}_{se}$ which a bridge deck is subjected to in an air stream of velocity U

and density ρ, is given as (Jain, *et al*. 1996a, b, Sarkar, *et al*. 1994, Singh, *et al*. 1995):

$$\boldsymbol{f}_{se} = \begin{Bmatrix} L_{se} \\ M_{se} \\ D_{se} \end{Bmatrix} = \begin{bmatrix} 0.5\rho U^2 B & 0 & 0 \\ 0 & 0.5\rho U^2 B^2 & 0 \\ 0 & 0 & 0.5\rho U^2 B \end{bmatrix}$$

$$\begin{bmatrix} KH_1^*/U & KH_2^*B/U & KH_5^*/U & K^2H_4^*/B & K^2H_3^* & K^2H_6^*/B \\ KA_1^*/U & KA_2^*B/U & KA_5^*/U & K^2A_4^*/B & K^2A_3^* & K^2A_6^*/B \\ KP_5^*/U & KP_2^*B/U & KP_1^*/U & K^2P_6^*/B & K^2P_3^* & K^2P_4^*/B \end{bmatrix} \begin{Bmatrix} \dot{h} \\ \dot{\alpha} \\ \dot{p} \\ h \\ \alpha \\ p \end{Bmatrix} \quad (1)$$

where L_{se}, D_{se} and M_{se} are aeroelastic (self-excited) lift, drag and pitching moment, respectively, $K=B\omega/U$ is the reduced frequency, ω=circular frequency of oscillation; H_i^*, A_i^* and P_i^* ($i=1, 2,\ldots, 6$) are the flutter derivatives determined experimentally from wind tunnel tests on an aeroelastic model of the bridge deck.

2.1. Unsteady aerodynamic modeling

Since the aeroelastic forces depend on reduced frequency, they are transformed into Laplace domain to facilitate the application of time domain approach. For this purpose, the aeroelastic forces are approximated as a common rational function.

The main difficulty in modeling an aeroelastic system for design lies in the representation of the unsteady aerodynamic loads. The unsteady aerodynamic forces, causing oscillatory motions of a section model in an incompressible flow, were first derived by Theodorsen (1935). Later, Jones (1941) presented the rational fraction approximation of the so called generalised Theodorsen Function. An approach, known as classical approach to flutter analysis which was first put forth by Bisplinghoff, *et al*. (1955), was based on aerodynamic influence coefficient matrices. These matrices were computed for simple harmonic motion at discrete values of reduced frequencies. In the evaluation of unsteady aerodynamic forces due to arbitrary motions, Edwards (1979) opened the way for calculating the aerodynamic influence coefficients in the Laplace domain (s-plane).

The self-excited forces due to unsteady wind force $\boldsymbol{f}_{se}$ can be represented by a ratio of polynomials in Laplace variable s. Generally, the wind forces are determined only for pure oscillatory motion of a structure, such as a lifting surface. For a casual, stable and linear system, analytic $\boldsymbol{f}_{se}(s)$ can be directly deduced from $\boldsymbol{f}_{se}(i\omega)$ which is obtained from an oscillatory theory. This is realized by approximating each term of the wind force matrix $\boldsymbol{f}_{se}(i\omega)$ by a rational polynomial in $(i\omega)$ and, then solving for the coefficients of the polynomial preferably by nonlinear least-squares fit with measured oscillatory wind forces at a given frequency. The transfer function matrix $\boldsymbol{f}_{se}(s)$ is then obtained by the replacement $s=i\omega$. In practice, it is more convenient to use the nondimensional reduced frequency $K=\omega B/U$ because, the oscillatory dynamic data are generally available corresponding to the reduced frequencies. Then, the Laplace variable also becomes nondimensionalised such that

$r = sB/U = iK$; $i = \sqrt{-1}$. There have been many approaches to this process. The basic method applied here is that of Roger (1977) who formulated a rational function approximation for three dimensional subsonic aerodynamics by using a series of poles to represent the aerodynamic lags attributable to the wake. The poles are chosen to be the same for all elements of the transfer matrix. The success of the fit is dependent on the choice of the poles which in turn is based on experience. The parameters of the function are determined by the least-squares technique. Another approach similar in many ways to the rational function approximation of Roger (1977) is that of Dowell (1980) who used a series of decaying exponentials in the time domain which in Laplace domain is represented as a series of simple poles. Peterson and Crawley (1988) applied Newton-Raphson gradient optimization process to solve for the lag parameters of the Dowell's exponential series in time domain. They included the numerator and denominator coefficients of the transfer function as the free parameters for optimization. Karpel (1982) developed a new minimum-state method for efficient rational function approximation of unsteady aerodynamic forces. He demonstrated it to result in a considerable lower order model relative to other methods of a comparable accuracy. But, because of the iterative feature of the method, it requires complicated computer routines and consumes more processor time. Tiffany and Adams (1987) used a nongradient nonlinear optimization process to select the values of the lag parameters in the least-squares formulation. The process resulted in a loss of accuracy and an erratic behaviour of the objective function with many number of lag states.

2.2. Rational function approximation of flutter derivatives

The rational function approximation presented by Roger (1977), and commonly used by Bucher and Lin (1988), Boonyapinyo, *et al*. (1999), Chen, *et al*. (2000a, b), Chen and Kareem (2002), is used in the present study. The form of rational function is given by:

$$\boldsymbol{f}_{se}(r) = \boldsymbol{a}_1^* + \boldsymbol{a}_2^* r + \boldsymbol{a}_3^* r^2 + \sum_{l=1}^{l=m_1} r \frac{\boldsymbol{a}_{l+3}^*}{r + b_l} \tag{2}$$

where $\boldsymbol{f}_{se}$ = unsteady aerodynamic matrix; $\boldsymbol{a}_1^*$, $\boldsymbol{a}_2^*$, $\boldsymbol{a}_3^*$, $\boldsymbol{a}_{l+3}^*$ = frequency independent coefficient matrices to be obtained from the known values of flutter derivatives by curve fitting and applying nonlinear least-squares method, and $l = 1, 2, \ldots, m_1$. The value of m_1 may be taken from 2 to 6. It also determines the number of lag terms and influences the convergence of the function. r is a nondimensional Laplace variable. The first term of the right hand side expression represents the noncirculatory static-aerodynamics. The second term represents the aerodynamic damping whereas, the third term represents the aerodynamic mass. The rational term accounts well for the nonlinearity and unsteadiness in the flow, and represents a lag from the velocity of oscillation. The poles which denote lag terms in the time domain are common for all the elements of $\boldsymbol{f}_{se}(s)$ thereby the number of supplementary aerodynamic states (explained in Subsection 4.3) are considerably reduced. The value of the lag parameter b approximates a time delay in the motion of the model. The accuracy of the approximation crucially depends on b, the values of which must be positive for the stability of the transfer function. When the inverse Laplace transform is applied on $\boldsymbol{f}_{se}$(s), the approximate aerodynamic unit impulse response matrix is obtained. Upon taking the convolution integral of the unit impulse response with the transient structural motion $\mathbf{z}(t)$, the approximate transient air force becomes available in the time domain.

Eq. (2) in terms of non-dimensional Laplace domain r is expressed as:

$$\begin{Bmatrix} \overline{L_{se}} \\ \overline{D_{se}} \\ \overline{M_{se}} \end{Bmatrix} = \frac{1}{2}\rho U^2 \begin{bmatrix} B & 0 & 0 \\ 0 & B & 0 \\ 0 & 0 & B^2 \end{bmatrix} \begin{bmatrix} K^2(iH_1^* + H_4^*) & K^2(iH_5^* + H_6^*) & K^2(iH_2^* + H_3^*) \\ K^2(iP_5^* + P_6^*) & K^2(iP_1^* + P_4^*) & K^2(iP_2^* + P_3^*) \\ K^2(iA_1^* + A_4^*) & K^2(iA_5^* + A_6^*) & K^2(iA_2^* + A_3^*) \end{bmatrix} \begin{Bmatrix} \left(\frac{\bar{h}}{B}\right) \\ \left(\frac{\bar{p}}{B}\right) \\ \bar{\alpha} \end{Bmatrix} \tag{3}$$

The rational function approximation of the self-excited forces in Laplace domain r is achieved by expressing the second matrix on the right hand side of Eq. (3) as:

$$\begin{bmatrix} K^2(iH_1^* + H_4^*) & K^2(iH_5^* + H_6^*) & K^2(iH_2^* + H_3^*) \\ K^2(iP_5^* + P_6^*) & K^2(iP_1^* + P_4^*) & K^2(iP_2^* + P_3^*) \\ K^2(iA_1^* + A_4^*) & K^2(iA_5^* + A_6^*) & K^2(iA_2^* + A_3^*) \end{bmatrix} = \boldsymbol{a}_1^* + \boldsymbol{a}_2^* r + \boldsymbol{a}_3^* r^2 + \sum_{l=1}^{l=m_1} r\frac{\boldsymbol{a}_{l+3}^*}{r + b_l} \tag{4}$$

On equating the imaginary and real terms, Eq. (4) breaks into the following forms:

$$H_1^* = \frac{1}{K}\left[a_2^* + \sum_{l=1}^{m_1} \frac{a_{l+3}^*}{b_l^2 + K^2} b_l\right] \tag{5a}$$

$$H_4^* = \left[\frac{a_1^*}{K^2} - a_3^* + \sum_{l=1}^{m_1} \frac{a_{l+3}^*}{b_l^2 + K^2}\right] \tag{5b}$$

Eqs. (5) are equivalent to the expressions given in Eqs. (16) and (17) of Bucher and Lin (1988), and Eqs. (47) and (48) of Scanlan, *et al*. (1974). Similar expressions can be written for all the other flutter derivatives.

The best fit parameters a_i^* (i=1, …, m_1+3) of Eqs. (5) have been determined by the nonlinear least-squares fit using Levenberg-Marquardt method (Marquardt 1963). The method is well elaborated in many references on regression or data reduction techniques, such as in Bevington (1969, Chap. 11) and Press, *et al*. (1992, Chap. 15).

The values of parameter b_l (l=1, …, m_1) may be kept fixed arbitrarily to ensure convergence and reduce the number of supplementary aerodynamic states. The arbitrary selection of the value of b does not make a great difference in the aerodynamic process and structural modes. However, to ensure system stability, parameter b must be greater than zero and should be restricted in the range of frequencies over which data is available (Fujino, *et al*. 1995).

3. Aerodynamic force discretisation

Eq. (3) represents uniformly distributed aeroelastic forces per unit length of the bridge deck. To implement finite element solution procedure for the structure, the forces are discretised at the element ends. In this discretisation, one-half of the total forces acting on an element are lumped at

its both ends.

As it is usually done in the scientific literature, and without loosing much accuracy, the aerodynamic forces acting only on the bridge deck have been considered for flutter analysis of the bridge deck and, aerodynamic forces on the pylons and cables have been ignored in this analysis.

3.1. Member aeroelastic matrices

The vector of lumped self-excited forces, after incorporating Eq. (4), is given as (Chen, *et al*. 2000a, b, Boonyapinyo, *et al*. 1999):

$$\begin{Bmatrix} L_{se} \\ M_{se} \\ D_{se} \end{Bmatrix}_{end} = \frac{1}{2}\rho U^2 \left(\tilde{\boldsymbol{a}}_1 + \tilde{\boldsymbol{a}}_2 r + \tilde{\boldsymbol{a}}_3 r^2 + \sum_{l=1}^{m_1} \tilde{\boldsymbol{a}}_{l+3} \frac{r}{r+b_l} \right) \begin{Bmatrix} \bar{h} \\ \bar{p} \\ \bar{\alpha} \end{Bmatrix} \tag{6}$$

where the matrices $\tilde{\boldsymbol{a}}_1$, $\tilde{\boldsymbol{a}}_2$, $\tilde{\boldsymbol{a}}_3$ and $\tilde{\boldsymbol{a}}_{l+3}$, $(l=1, \ldots, m_1)$ are 3×3 coefficient matrices obtained for each element of the deck. The elements of these matrices are as follows:

$$\tilde{\boldsymbol{a}}_1 = \begin{bmatrix} a^*_{1_{11}}\frac{L}{2} & a^*_{1_{12}}\frac{L}{2} & a^*_{1_{13}}\frac{BL}{2} \\ a^*_{1_{21}}\frac{L}{2} & a^*_{1_{22}}\frac{L}{2} & a^*_{1_{23}}\frac{BL}{2} \\ a^*_{1_{31}}\frac{BL}{2} & a^*_{1_{32}}\frac{BL}{2} & a^*_{1_{33}}\frac{B^2L}{2} \end{bmatrix}; \qquad \tilde{\boldsymbol{a}}_1 = \begin{bmatrix} a^*_{2_{11}}\frac{L}{2} & a^*_{2_{12}}\frac{L}{2} & a^*_{2_{13}}\frac{BL}{2} \\ a^*_{2_{21}}\frac{L}{2} & a^*_{2_{22}}\frac{L}{2} & a^*_{2_{23}}\frac{BL}{2} \\ a^*_{2_{31}}\frac{BL}{2} & a^*_{2_{32}}\frac{BL}{2} & a^*_{2_{33}}\frac{B^2L}{2} \end{bmatrix};$$

$$\tilde{\boldsymbol{a}}_3 = \begin{bmatrix} a^*_{3_{11}}\frac{L}{2} & a^*_{3_{12}}\frac{L}{2} & a^*_{3_{13}}\frac{BL}{2} \\ a^*_{3_{21}}\frac{L}{2} & a^*_{3_{22}}\frac{L}{2} & a^*_{3_{23}}\frac{BL}{2} \\ a^*_{3_{31}}\frac{BL}{2} & a^*_{3_{32}}\frac{BL}{2} & a^*_{3_{33}}\frac{B^2L}{2} \end{bmatrix}; \qquad \tilde{\boldsymbol{a}}_{1+3} = \begin{bmatrix} a^*_{l+3_{11}}\frac{L}{2} & a^*_{l+3_{12}}\frac{L}{2} & a^*_{l+3_{13}}\frac{BL}{2} \\ a^*_{l+3_{21}}\frac{L}{2} & a^*_{l+3_{22}}\frac{L}{2} & a^*_{l+3_{23}}\frac{BL}{2} \\ a^*_{l+3_{31}}\frac{BL}{2} & a^*_{l+3_{32}}\frac{BL}{2} & a^*_{l+3_{33}}\frac{B^2L}{2} \end{bmatrix}; \tag{7}$$

The deck members of the cable-stayed bridge were discretised into space frame elements each having 12 degrees of freedom. The elements of the matrices $\tilde{\boldsymbol{a}}_1$, $\tilde{\boldsymbol{a}}_2$, $\tilde{\boldsymbol{a}}_3$ and $\tilde{\boldsymbol{a}}_{l+3}$, $(l=1, \ldots, m_1)$ obtained from Eq. (7), constitute 12×12 matrices $\boldsymbol{a}^e_1$, $\boldsymbol{a}^e_2$, $\boldsymbol{a}^e_3$ and $\boldsymbol{a}^e_{l+3}$ for each structural element. The nonzero elements of a typical coefficient matrix, $\boldsymbol{a}^e_j$ (12×12), $(j=1, \ldots, m_1+3)$ for an element, are given as:

$$a_j(2,2) = a_j(8,8) = a^*_{j_{11}}\frac{L}{2} \tag{8a}$$

$$a_j(2,3) = a_j(8,9) = a^*_{j_{12}}\frac{L}{2} \tag{8b}$$

$$a_j(2,4) = a_j(8,10) = a^*_{j_{13}}\frac{BL}{2} \tag{8c}$$

$$a_j(3,2) = a_j\ (9,8) = a_{j_{21}}^* \frac{L}{2} \tag{8d}$$

$$a_j(3,3) = a_j\ (9,9) = a_{j_{22}}^* \frac{L}{2} \tag{8e}$$

$$a_j(3,4) = a_j\ (9,10) = a_{j_{23}}^* \frac{BL}{2} \tag{8f}$$

$$a_j(4,2) = a_j\ (10,8) = a_{j_{31}}^* \frac{BL}{2} \tag{8g}$$

$$a_j(4,3) = a_j\ (10,9) = a_{j_{32}}^* \frac{BL}{2} \tag{8h}$$

$$a_j(4,4) = a_j\ (10,10) = a_{j_{33}}^* \frac{B^2 L}{2} \tag{8i}$$

The set of matrices $\boldsymbol{a}_j^e$ ($j=1, \ldots, m_1+3$) form together the coefficients of rational function approximation of the self-excited force vector for each element of the deck.

3.2. Global self-excited force vector

Having obtained the coefficient matrices, $\boldsymbol{a}_j^e$, ($j=1, \ldots, m_1+3$) for each element of the deck, the assembly of the matrices is carried out to obtain the global matrices $\boldsymbol{a}_j(n_1 \times n_1)$, where n_1 = degrees of freedom of the structure. The global self-excited force vector $\overline{\boldsymbol{F}}_{se}$ in the Laplace domain is obtained as:

$$\overline{\boldsymbol{F}}_{se} = \frac{1}{2}\rho U^2 \left(\boldsymbol{a}_1 + \boldsymbol{a}_2 r + \boldsymbol{a}_3 r^2 + \sum_{l=1}^{m_1} \boldsymbol{a}_{l+3} \frac{r}{r+b_l} \right) \boldsymbol{z}(s) \tag{9}$$

where $\boldsymbol{z}(s)$ = displacement vector ($n_1 \times 1$) in the Laplace domain.

4. Modal state-space equation

4.1. Modal equation of motion

The governing equation of motion, for n_1 degrees of freedom system having mass, damping and stiffness matrices $\boldsymbol{m}$, $\boldsymbol{c}$ and $\boldsymbol{k}$ respectively, and, the nodal physical response vector $\boldsymbol{z}(t)$, is:

$$\boldsymbol{m}\ddot{\boldsymbol{z}} + \boldsymbol{c}\dot{\boldsymbol{z}} + \boldsymbol{k}\boldsymbol{z} = \boldsymbol{f}_{se}(t) \tag{10}$$

The response, $\boldsymbol{z}$ is transformed in terms of spatial, $\boldsymbol{\Phi}(x, y, z)$ and temporal components, $\boldsymbol{q}(t)$ as:

$$z(x, y, z, t) = \boldsymbol{\Phi}(x, y, z)\boldsymbol{q}(t) = \sum_{j=1}^{n} \phi_j(x, y, z) q_j(t) \tag{11}$$

where n = number of modes selected ($n \le n_1$). Inserting Eq. (11) into Eq. (10) and premultiplying it by $\boldsymbol{\Phi}^T$ and, assuming that the bridge is modally damped, then the modal equation of motion is written as:

$$\mathbf{M}\ddot{\boldsymbol{q}} + \mathbf{C}\dot{\boldsymbol{q}} + \mathbf{K}\boldsymbol{q} = \mathbf{F}_{se}(t) \tag{12}$$

where the upright bold $\mathbf{M} = \boldsymbol{\Phi}^T\boldsymbol{m}\boldsymbol{\Phi}$= modal mass matrix; $\mathbf{C} = \boldsymbol{\Phi}^T\boldsymbol{c}\boldsymbol{\Phi}$= modal damping matrix $= 2\zeta_j\omega_j M_j$; ζ_j, ω_j and $M_j = j$ th mode damping ratio, frequency and mass respectively; $\mathbf{K} = \boldsymbol{\Phi}^T\boldsymbol{k}\boldsymbol{\Phi}$= modal stiffness matrix $= \omega_j^2 M_j$; $\mathbf{F_{se}} = \boldsymbol{\Phi}^T\boldsymbol{f}_{se}$ = modal self-excited force vector.

4.2. Modal equation of motion in the Laplace domain

Eq. (12) is written in the Laplace domain as:

$$\mathbf{M}s^2\boldsymbol{q}(s) + \mathbf{C}s\boldsymbol{q}(s) + \mathbf{K}\boldsymbol{q}(s) = \boldsymbol{\Phi}^T\bar{\mathbf{F}}_{se}(s) \tag{13}$$

The Laplace-transformed self-excited force vector, $\bar{\mathbf{F}}_{se}$ is already available in Eq. (9). Eq. (13), in conjunction with Eq. (9) and with substitution $\boldsymbol{z}(x, y, z, s) = \boldsymbol{\Phi}(x, y, z)\ \boldsymbol{q}(s)$, is given as:

$$\mathbf{M}s^2\boldsymbol{q}(s) + \mathbf{C}s\boldsymbol{q}(s) + \mathbf{K}\boldsymbol{q}(s) = \boldsymbol{\Phi}^T\left[\frac{1}{2}\rho U^2\left(\boldsymbol{a}_1 + \boldsymbol{a}_2 r + \boldsymbol{a}_3 r^2 + \sum_{l=1}^{m_1}\boldsymbol{a}_{l+3}\frac{r}{r+b_l}\right)\boldsymbol{\Phi}\boldsymbol{q}(s)\right] \tag{14}$$

Now, following substitutions are made: $r = sB/U$ and $\boldsymbol{\Phi}^T\boldsymbol{a}_j\boldsymbol{\Phi} = \mathbf{A}_j$; where $\mathbf{A}_j (j = 1, \ldots, m_1 + 3)$ are termed as modal aeroelastic matrices. Then, bringing the right hand side terms of Eq. (14) to the left and assigning new notations as: $\bar{\mathbf{M}} = \mathbf{M} - \frac{1}{2}\rho B^2\mathbf{A}_3$; $\bar{\mathbf{C}} = \mathbf{C} - \frac{1}{2}\rho UB\mathbf{A}_2$; $\bar{\mathbf{K}} = \mathbf{K} - \frac{1}{2}\rho U^2\mathbf{A}_1$; where $\bar{\mathbf{M}}, \bar{\mathbf{C}}$ and $\bar{\mathbf{K}}$ are called aeroelastically modified modal mass, modal damping and modal stiffness matrices, respectively. The final form of modal equations of motion in the Laplace domain is obtained as:

$$\left(\bar{\mathbf{M}}s^2 + \bar{\mathbf{C}}s + \bar{\mathbf{K}} - \frac{1}{2}\rho U^2\sum_{l=1}^{m_1}\mathbf{A}_{l+3}\frac{s}{s + \dfrac{b_l U}{B}}\right)\boldsymbol{q}(s) = \mathbf{0} \tag{15}$$

4.3. Modal state-space form of equation

The state–space model, for describing the response of a bridge, has several significant mathematical advantages. The recasting of system equations in the state-space form enables the use of tools based on linear system theory for response analysis. In addition, the structural and aerodynamic coupling effects can be automatically included in the computation. To recast the equation of motion in state-space form, the rational terms in Eq. (15) need to be modeled as aerodynamic state coordinates. Thus, introducing new supplementary coordinates as:

$$\boldsymbol{q}_{se\,l}(s) = \frac{\mathbf{A}_{l+3}s}{s + \dfrac{b_l U}{B}}\boldsymbol{q}(s) \tag{16}$$

which can be rewritten as:

$$s\boldsymbol{q}_{se\,l}(s) + \frac{b_l U}{B}\boldsymbol{q}_{se\,l}(s) = \mathbf{A}_{l+3}s\boldsymbol{q}(s) \tag{17}$$

where $\boldsymbol{q}_{se\,l}$ (l=1, …, m_1)=new supplementary aerodynamic state vectors. These vectors represent the unsteady aerodynamic states. The inverse Laplace transform of Eq. (17) can be written as:

$$\dot{\boldsymbol{q}}_{se\,l} = \mathbf{A}_{l+3}\dot{\boldsymbol{q}} - \frac{b_l U}{B}\boldsymbol{q}_{se\,l}(t) \qquad l=1, \ldots, m_1 \tag{18}$$

Now taking the inverse Laplace transform of Eq. (15), we get the modal equation of motion in the time domain as:

$$\overline{\mathbf{M}}\ddot{\boldsymbol{q}} + \overline{\mathbf{C}}\dot{\boldsymbol{q}} + \overline{\mathbf{K}}\boldsymbol{q} - \frac{1}{2}\rho U^2 \sum_{l=1}^{m_1} \boldsymbol{q}_{se\,l}(t) = \mathbf{0} \tag{19}$$

In conjunction with Eq. (18), Eq. (19) can be expressed in state-space form as:

$$\begin{Bmatrix} \dot{\boldsymbol{q}} \\ \ddot{\boldsymbol{q}} \\ \dot{\boldsymbol{q}}_{se\,1} \\ . \\ . \\ . \\ \dot{\boldsymbol{q}}_{se\,m_1} \end{Bmatrix} = \begin{bmatrix} \mathbf{0} & \mathbf{I} & \mathbf{0} & \cdots & \mathbf{0} \\ -\overline{\mathbf{M}}^{-1}\overline{\mathbf{K}} & -\overline{\mathbf{M}}^{-1}\overline{\mathbf{C}} & \frac{1}{2}\rho U^2 \overline{\mathbf{M}}^{-1} & \cdots & \frac{1}{2}\rho U^2 \overline{\mathbf{M}}^{-1} \\ \mathbf{0} & \mathbf{A}_4 & -\frac{Ub_1\mathbf{I}}{B} & \cdots & \mathbf{0} \\ . & . & . & \cdots & . \\ . & . & . & \cdots & . \\ . & . & . & \cdots & . \\ \mathbf{0} & \mathbf{A}_{3+\mathbf{m}_1} & \mathbf{0} & \cdots & -\frac{Ub_{m_1}\mathbf{I}}{B} \end{bmatrix} \begin{Bmatrix} \boldsymbol{q} \\ \dot{\boldsymbol{q}} \\ \boldsymbol{q}_{se\,1} \\ . \\ . \\ . \\ \boldsymbol{q}_{se\,m_1} \end{Bmatrix} \tag{20}$$

Eq. (20) can be written symbolically as:

$$\dot{\boldsymbol{Y}} = \boldsymbol{A}\boldsymbol{Y} \tag{21}$$

Eq. (21) is linear and frequency independent which is used to analyse the structural response. Matrix $\boldsymbol{A}$ is an aeroelastically modified modal state matrix. It is obvious that the technique of rational function approximation of self-excited forces can be used for analyzing the system with frequency dependent parameters in the time domain approach. In bridge aerodynamics, flutter and buffeting responses can also be analysed in the time domain by the same numerical formulation (Chen, *et al*. 2000a). It is evident from Eq. (20) that matrix $\boldsymbol{A}$ is a function of wind speed U, wind mass density ρ, rational function coefficients a^* as well as bridge deck element dimensions B (width) and L (length). The main advantage of applying this approach is that all eigenvalues corresponding to the natural modes of the structure at a given wind velocity can be computed without iteration.

5. Solution for eigenvalues and damping

At a given wind velocity, the solution of Eq. (21) can be given in the form:

$$\boldsymbol{Y}(t) = e^{\lambda t}\boldsymbol{V} \tag{22}$$

where λ is scalar and $\boldsymbol{V}$ is vector. Introducing Eq. (22), Eq. (21) results in

$$\boldsymbol{AV}=\lambda \boldsymbol{V} \tag{23}$$

Eq. (23) is a standard eigenvalue problem. For n structural generalised coordinates (or modes) the eigenvalues of $\boldsymbol{A}$ are n complex conjugate pairs [λ_j, λ_{j+1} ($j = 1, 3, \ldots, 2n-1$)] given as:

$$\lambda_j, \lambda_{j+1} = \lambda_{R_j} \pm i\lambda_{I_j} = \zeta_j \omega_j \pm i\omega\sqrt{(1-\zeta_j^2)} \tag{24}$$

where $i = \sqrt{-1}$. However, some structural eigenvalues might be real, as well, which correspond to overdamped modes. Such a case is excluded from the present investigation. The remaining eigenvalues $2n+1$, $2n+2$, ..., $2n+nm_1$ are attributable to the fluid behavior and are generally real valued (Boonyapinyo, *et al*. 1999). However, some of them may be complex depending on the values of the constant b_l, ($l = 1, ..., m_1$) in the denominator of the rational term of Eq. (15). It is noted that due to the introduction of the supplementary unsteady aerodynamic states, Eq. (19) results into the supplementary solution and, only modes relating to structural motion are useful for structural response analysis.

By analogy with the properties of a single degree of freedom system, the natural frequency and modal damping ratio associated with an underdamped mode are defined as:

$$\omega_j = |\lambda_j| = \sqrt{\lambda_{R_j}^2 + \lambda_{I_j}^2}; \tag{25}$$

$$\zeta_j = -\frac{\mathrm{Re}(\lambda_j)}{|\lambda_j|} \tag{26}$$

where $j = 1, 3, ..., 2n-1$. The above value of ζ contains both the structural plus aerodynamic damping. Thus the combined structural plus aerodynamic system's logarithmic decrement δ_j is given by:

$$\delta_j \approx 2\pi\zeta_j = -\frac{2\pi\lambda_{Rj}}{\sqrt{\lambda_{Rj}^2 + \lambda_{Ij}^2}} \tag{27}$$

6. Application to example bridge

6.1. Constitution of state matrix $\boldsymbol{A}$

In this study, a long span cable-stayed bridge of main-span 1020 m with two side-spans each of 375 m has been considered (Fig. 1). The cross-section of the bridge deck which is of steel is shown in Fig. 2. Each tower 223.6 m high carries 25 pairs of cables both from side-span as well as from main-span. The spacing of the cable-tower anchorage is 2 m while the spacing of cable-deck anchorage on the side span is 15 m, and that on main-span is 20 m. The finite element discretisation and free vibration analysis of the example bridge were performed by a computer programme 'EIGEN' written in MATLAB (1996). The system mass ($\boldsymbol{m}$) and stiffness ($\boldsymbol{k}$) matrices of the order 1626×1626 obtained originally were condensed to the order 588×588 using the Guyan (1965) reduction technique. The active degrees of freedom corresponding to h, p and α were selected on the deck nodes only. Numbers of active nodes selected were 196 (588 dof) out of which 48 nodes were in each side span and 100 nodes in the central span. Active nodes selected were symmetrical with respect to the mid-span of the bridge. The first six mode shapes of the cable-stayed bridge obtained from the free vibration analysis are presented in Fig. 3.

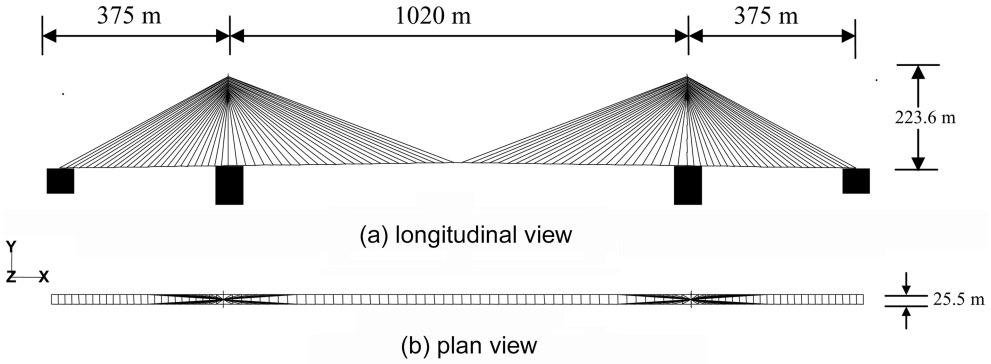

Fig. 1 Schematic view of long span cable-stayed bridge

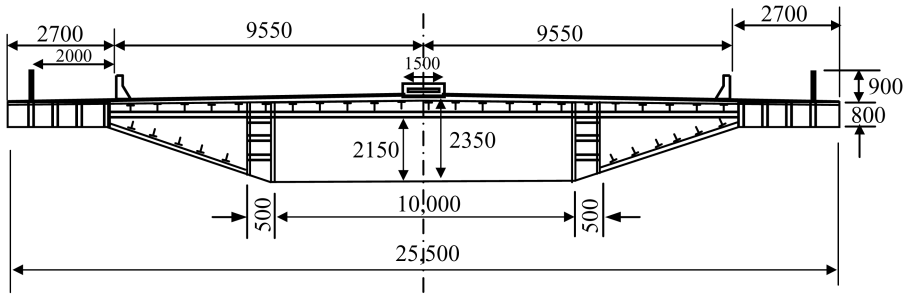

Fig. 2 Cross-section of the bridge deck under study

The wind tunnel tests were performed in a large size (2.0 m wide × 2.1 m high) boundary layer wind tunnel of the Indian Institute of Technology, Roorkee, India. The full set of eighteen flutter derivatives were extracted from the tests on the elastically suspended section model of the bridge deck section in smooth wind. The details of the tests may be found in Mishra (2005) and Mishra, *et al*. (2006). The rational function approximated flutter derivatives are given in Fig. 4. It is seen that the rational function approximates the flutter derivatives well.

In order to constitute the matrices of modal mass **M**, damping **C** and stiffness **K** and, the vector of modal self-excited force $\mathbf{F}_{se}$ for implementation in Eq. (12), first 100 eigenvalues and eigenvectors were taken from the free vibration analysis of the bridge system. 100 numbers of eigenvalues and eigenvectors are fairly a good number as most of the dynamic analyses of cable-stayed bridges seldom incorporate modes above 30. A constant modal damping ratio $\zeta = 1.5\%$ of critical was selected which is the normally adopted value in case of cable-stayed bridges (the value of for cable-stayed bridges reported in literature lies between 1% and 2%). The rational function coefficients a_l^* ($l = 1, ..., 7$), which are used in the development of the modal aeroelastic matrices $\mathbf{A}_j$ ($j = 1, ..., 7$), are based on the full set of 18 experimentally obtained flutter derivatives for the bridge deck under study**.** The size of the modal state matrix ***A*** depends upon the number of free vibration modes selected.

The matrices $\overline{\mathbf{M}}$, $\overline{\mathbf{C}}$ and $\overline{\mathbf{K}}$ are obtained from the definitions preceding Eq. (15). The values of b_l, ($l = 1, ..., m_1$) for $m_1 = 4$ were taken positive and kept fixed at 0.5, 2.0, 5.0 and 7.0. These arbitrary values of b do not affect appreciably the aerodynamic forces and process provided they are limited

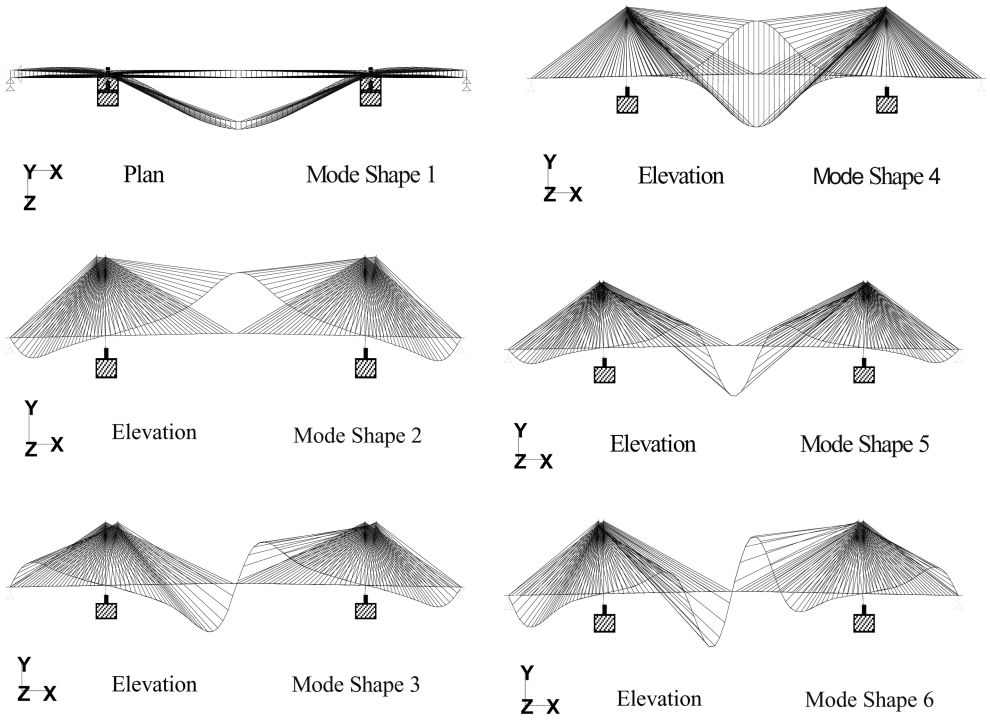

Fig. 3 First six mode shapes of the cable-stayed bridge

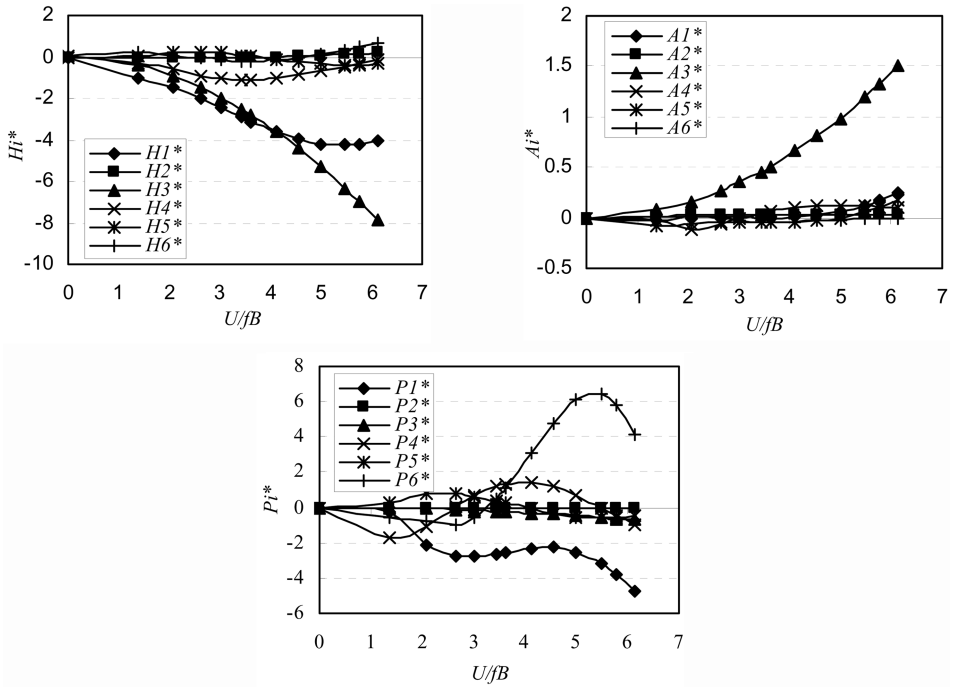

Fig. 4 Flutter derivatives for the bridge deck model

within the maximum free vibration frequency obtained from model testing (Xie and Xiang 1985, Boonyapinyo 1999). For the bridge deck under investigation, the maximum free vibration torsional frequency is 7.00 Hz. The mass density of air, is taken as 1.225 kg/m^3. For the first 100 natural modes selected the modal state matrix $\boldsymbol{A}$ obtained is of order 600×600.

6.2. Computation of eigenvalues

The MATLAB programme EIGEN was extended to generate the aeroelastically modified modal state matrix $\boldsymbol{A}$. The programme uses the 'eigs' command in conjunction with 'si' command available in MATLAB for the determination of the complex eigen values. The 'eigs' command uses the ARPACK library programme based on Arnoldi's (1951) method for solving the eigenproblem. To check the accuracy of the modes and frequencies, programme EIGEN was applied to compute

Table 1 Natural and wind induced frequencies at different wind velocities for the cable-stayed bridge

Mode no.	Natural frequency	Frequency at $U=0$	Frequency at $U=10$ m/s	Frequency at $U=20$ m/s
1	0.1572	0.1572	0.1569	0.1643
2	0.1673	0.1673	0.1678	0.1675
3	0.1917	0.1917	0.1923	0.1915
4	0.2799	0.2799	0.2806	0.2788
5	0.2961	0.2961	0.2971	0.2966
6	0.3345	0.3345	0.3351	0.3343
7	0.3376	0.3376	0.3385	0.3386
8	0.3613	0.3613	0.3622	0.3626
9	0.3788	0.3788	0.3797	0.3803
10	0.4045	0.4045	0.4051	0.4052
11	0.4128	0.4128	0.4136	0.4154
12	0.4330	0.4330	0.4339	0.4331
13	0.4376	0.4376	0.4384	0.4337
14	0.4402	0.4402	0.4417	0.4403
15	0.4478	0.4478	0.4486	0.4497
16	0.4576	0.4576	0.4588	0.4581
17	0.4781	0.4781	0.4788	0.4801
18	0.4839	0.4839	0.4847	0.4859
19	0.5048	0.5048	0.5053	0.5061
20	0.5061	0.5061	0.5068	0.5081
21	0.5569	0.5569	0.5577	0.5590
22	0.5581	0.5581	0.5586	0.5595
23	0.5702	0.5702	0.5708	0.5717
24	0.5705	0.5705	0.5710	0.5719
25	0.5892	0.5892	0.5899	0.5913

their values corresponding to wind velocities of 0, 10 and 20 m/s. The wind induced frequencies vis-a-vis natural frequencies up to first 25 modes are presented in Table 1.

It was considered appropriate to obtain frequencies and damping corresponding to the first 30 modes for the example bridge. From this point of view, the first 100 mode frequencies were computed from the programme but only first 30 modes were retained for presentation. The values of logarithmic decrement and undamped frequencies were calculated for a range of wind velocities starting from 0 m/s to 45 m/s at an increment of 5 m/s. From this computation, the range of wind velocity in which instability would occur was determined. Then, in the identified range the computation was carried out at a refined increment of U of 0.1 m/s.

7. Effect of aeroelastic forces on damping of the bridge

For a given mode, the logarithmic decrement is proportional to damping ratio of the mode. It is observed that for few lower modes up to 6, damping is almost constant at lower wind velocities up to 10 m/s (Fig. 5a). The curves depict that the prospective coupling modes have highly fluctuating damping and the curves change their slopes with increasing wind velocities. The change in slopes of these unstable modes is tremendous about their zero damping values. In general, the values of damping in the prospective coupling modes tend to decline with increasing wind velocity before their zero crossing. It is also observed that, by a flutter prone mode negative damping is attained at the point of frequency coupling. However, all modes except the coupled modes seem to have more or less same damping, the value of which increases with almost constant rate with increasing wind velocity. At a given wind velocity (before the onset of flutter), the values of damping go on decreasing with increasing mode numbers. However, after the onset of flutter (at zero damping), all the modes begin to lose their damping with varying rates. This aspect of the modes is revealed by the downward trends of the curves in Fig. 5a. It may be possible that all the modes would attain negative damping at higher wind velocities.

It is observed that between the two prospective coupling modes, the higher mode's damping becomes zero or negative. Further, the lower mode tends to catch the frequency of the higher mode. In other words, the higher mode extracts energy from the lower mode. This may be true for the few lower coupling modes in which one of the modes is losing damping.

8. Effect of aeroelastic forces on frequency of the bridge

As is seen from the curves of frequency vs. wind velocity (Fig. 5b), it can be said that the frequencies may increase or decrease with increase in the wind velocity. A closer look indicates that the frequencies of the modes, which do not have a proclivity to coupling, do not differ appreciably from their natural frequencies. The curves show a very minor increase in frequencies with increasing wind velocities, especially before the flutter speed is attained. This may be attributed to the stiffening of the stay cables due to structural nonlinear effects as oscillation proceeds under the drag of wind, since the structural nonlinear effects have already been included in the formation of the aeroelastically modified modal state matrix $\boldsymbol{A}$. Thereafter, the frequencies begin to decrease with increasing wind velocity, especially for the stable and higher modes.

A very interesting situation is shown by modes 1, 2 and 3. The paths of the companion modes are being interchanged after their coupling. This may be due to the exchange of energies between the companion modes. However, this fact needs to be verified by more such studies.

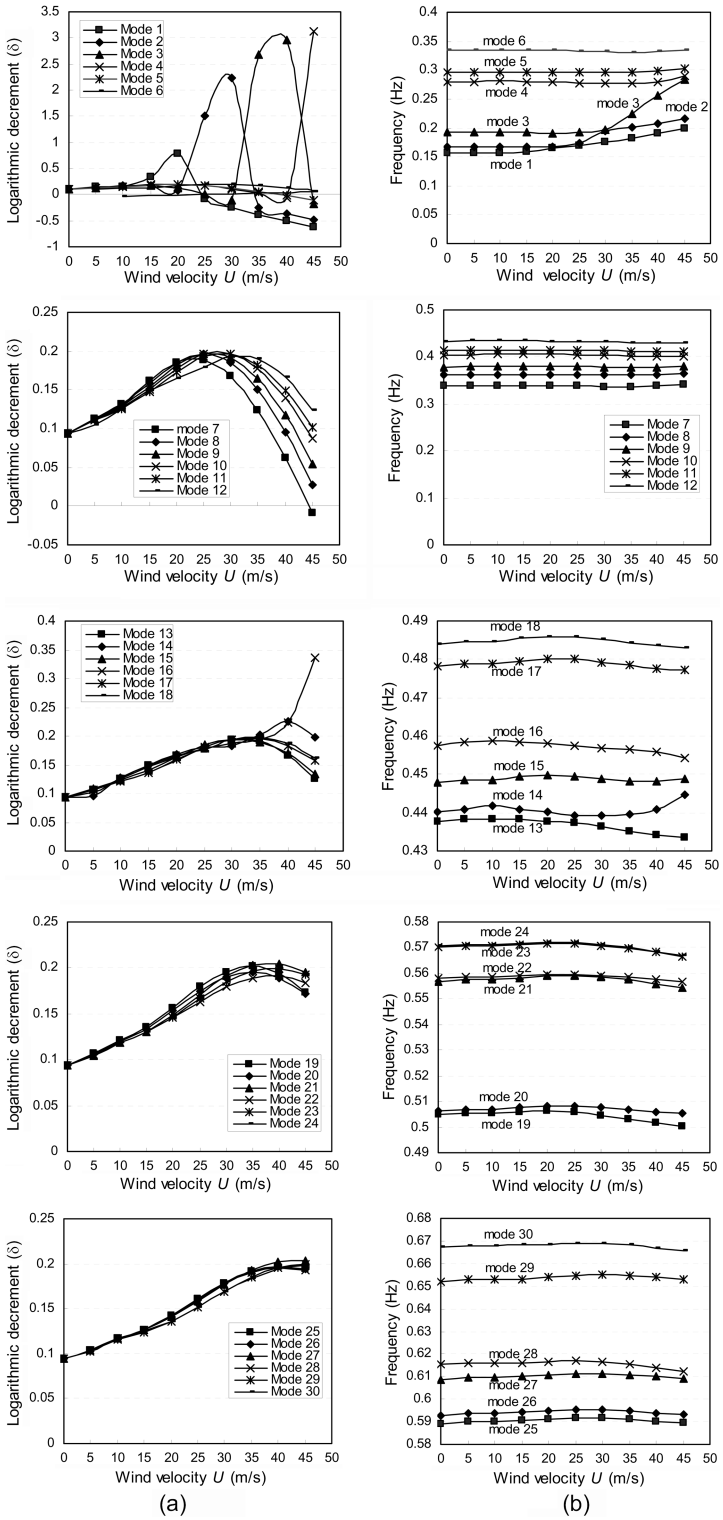

Fig. 5 Plots of (a) δ-U and (b) f-U curves for the first 30 modes

It is also observed that modes 1 and 2 unite to the same frequency at about 24 m/s wind velocity, and at the same wind velocity the damping of mode 1 also becomes negative. At this point of wind speed, flutter is bound to take place, since both the causes of instability exist.

9. Concluding remarks

This paper presents an application of the theory of modal state-space time domain stability analysis through rational function approximation of unsteady self-excited forces, and highlights the influence of wind on the structural damping and frequency of a long span cable-stayed bridge. Conclusions of this study which are revealed by this theory (though should not be generalised) are summarized below.

It is difficult to generalize a definite trend of frequency with wind. However, for this example, a closer look suggests that the frequencies of the modes do not differ appreciably from their natural frequencies at least for modes not showing tendency to coalesce in the flutter mode. For the stable and higher modes, especially before the critical flutter speed, a very minor increase in frequencies with wind speeds is observed. Thereafter, the frequencies begin to decrease with wind velocity. For the prospective coupling modes, the frequencies of these modes unite together giving a case of coupled flutter. In this process, lower mode strides to catch the frequency of higher modes.

The values of damping for a few lower modes are almost constant within a short range of wind velocity. In the vicinity of flutter critical wind speeds, these modes have highly fluctuating damping values. The higher modes have almost same value of damping which goes on increasing steadily even immediately after the onset of flutter and thereafter begins to crash**.** It may be possible that all the modes will attain negative damping at higher wind velocities with varying rates.

The necessary and sufficient condition for onset of flutter can be established at a wind velocity when, frequency coupling as well as negative damping of at least one of the modes occur.

Acknowledgements

The work described in this paper is a part of Ph. D. work of the first author. The authors of this paper greatly acknowledge the coordinator of the wind tunnel facility at the Indian Institute of Technology Roorkee, India and, also the parent Institute, NERIST of the first author for sponsoring him to pursue his Ph. D. work.

References

Arnoldi, W. E. (1951), "The principle of minimised iterations in the solutions of the matrix eigenvalue problem", *Quart. Appl. Math*., **9**, 17-29.

Bisplinghoff, R. L., Ashley, H. and Halfman, R. L. (1955), *Aeroelasticity*, Addison-Wesley Publishing Co. Inc., Cambridge, USA.

Bucher, C. G. and Lin, Y. K. (1988), "Stochastic stability of bridge considering coupled modes", *J. Eng. Mech.,* ASCE, **114**(12), 2055-2071.

Bevington, P. R. (1969), *Data Reduction and Error Analysis for the Physical Science*, McGraw-Hill Book Company, NY.

Boonyapinyo, V., Miyata, T. and Yamada, H. (1999), "Advanced aerodynamic analysis of suspension bridges by state space approach", *J. Struct. Eng.,* ASCE, **125**(12), 1357-1366.

Caracoglia, L. and Jones, N. P. (2003), "Time domain vs. frequency domain characteristics of aeroelastic forces

for bridge deck sections", *J. Wind Eng. Ind. Aerodyn*., **91**, 371-402.
Chen, X. and Kareem, A. (2002), "Advances in modeling of aerodynamic forces on bridge decks", *J. Eng. Mech.,* ASCE, **128**(11), 1193-1205.
Chen, X., Matsumoto, M. and Kareem, A. (2000a), "Time domain flutter and buffeting response analysis of bridges", *J. Eng. Mech.,* ASCE, **126**(1), 7-16.
Chen, X., Matsumoto, M. and Kareem, A. (2000b), "Aerodynamic coupling effects on the flutter and buffeting of bridges", *J. Eng. Mech.,* ASCE, **126**(1), 17-26.
Dowell, E. H. (1980), "A simple approach of converting frequency domain aerodynamics to the time domain", NASA TM-81844.
Edwards, J. H. (1979), "Application of Laplace transform methods to airfoil motion and stability calculations", *AIAA Paper* 70-0772.
Fujino, Y., Wilde, K., Masukawa, J. and Bhartia, B. (1995), "Rational function approximation of aerodynamics forces on bridge deck and its application to active control of flutter", *Proc. 9ICWE, New Delhi*, India, 994-1005.
Guyan, R. J. (1965), "Reduction of stiffness and mass matrices", *J. AIAA*, **3**(2), 380.
Hjorth-Hansen, E. (1992), "Section model tests", *Proc. of 1st Int. Symp. on Aerodynamics of Large Bridges,* A. Larsen (ed.), Balkema, Rotterdam, 95-112.
Jain, A., Jones, N. P. and Scanlan, R. H. (1996a), "Coupled flutter and buffeting analysis of long-span bridges", *J. Struct. Eng.,* ASCE, **122**(7), 716-725.
Jain, A., Jones, N. P. and Scanlan, R. H. (1996b), "Coupled aeroelastic and aerodynamic response analysis of long-span bridges", *J. Wind Eng. Ind. Aerodyn*., **60**, 69-80.
Jones, N. P. and Scanlan, R. H. (1991), "Issues in the multimode aeroelastic analysis of cable-stayed bridges", *Proceedings of International Workshop on Technology*, for Hong Kong's Infrastructure, 281-290.
Jones, N. P. and Scanlan, R. H. (2001), "Theory and full bridge modeling of wind response of cable supported bridges", *J. Bridge. Eng.,* ASCE, **6**(6), 365-375.
Jones, R. T. (1941), "The unsteady lift of a wing of finite aspect ratio", NACA Rept., 681.
Karpel, M. (1982), "Design for active flutter suppression and gust alleviation using state-space aeroelastic modeling", *J. Aircraft*, **19**(3), 221-227.
Katsuchi, H., Jones, N.P., Scanlan, R. H. and Akiyama, H. (1998), "Multimode flutter and buffeting analysis of the Akashi-Kaikyo Bridge", *J. Wind Eng. Ind. Aerodyn*., **77&78**, 431-441.
Lin, Y. K. and Yang, J. N. (1983), "Multimode bridge response to wind excitations", *J. Eng. Mech.,* ASCE, **109**(2), 586-603.
Marquardt, D. W. (1963), "An algorithm for least-squares estimation of nonlinear parameters", *J. Soc. Ind. Appl. Math*., **11**(2), 431-441.
MATLAB (1996), Using Matlab version 5, The Mathworks Inc, Nattick, MA, USA, [http://www.mathworks.com].
Mishra, S. S. (2005), "Effect of wind drag on flutter of long span cable-stayed bridges", Ph.D. Thesis, Indian Institute of Technology Roorkee, India.
Mishra, S. S., Kumar, K. and Krishna, P. (2006), "Identification of 18 flutter derivatives by covariance driven stochastic subspace method", *Wind Struct.*, **9**(2), 159-178.
Peterson, L. D. and Crawley, E. F. (1988), "Improved exponential time series approximations of unsteady aerodynamic operators", *J. Aircraft*, **25**(2).
Press, W. H., Teukolsky, S. A., Vellerling, W. T. and Flannery, B. P. (1992), *Numerical Recipes in FORTRAN*, 2nd ed., Cambridge University Press.
Roger, K. (1977), "Airplane math modeling methods for active control design", *Structural Aspects of Active Control*, Agard-CP-228.
Sarkar, P. P., Jones, N. P. and Scanlan, R. H. (1994), "Identification of aeroelastic parameters of flexible bridges", *J. Eng. Mech.,* ASCE, **120**(8), 1718-1742.
Scanlan, R. H. (1978), "The action of flexible bridges under wind. I: Flutter theory", *J. Sound Vib*., **60**(2), 187-199.
Scanlan, R. H. (1993), "Problematics in formulation of wind-force models for bridge decks", *J. Eng. Mech.,* ASCE, **119**(7), 1353-1375.
Scanlan, R. H., Beliveau, J. G., and Budlong, K. S. (1974), "Indicial aerodynamic functions for bridge decks", *J.*

Eng. Mech., ASCE, **100**(EM 4), 657-672.
Scanlan, R. H. and Jones, N. P. (1990), "Aeroelastic analysis of cable stayed bridges", *J. Struct. Eng.,* ASCE, **116**(2), 279-297.
Singh, L., Jones, N. P., Scanlan, R. H. and Lorendeaux, O. (1995), "Simultaneous identification of 3-dof aeroelastic parameters", *Proceedings of 9th International Conference on Wind Engineering*, New Delhi, India. Wiley Eastern Ltd., 872-881.
Tanaka, H., Yamamura, N. and Tatsumi, M. (1992), "Coupled mode flutter analysis using flutter derivatives", *J. Wind Eng. Ind. Aerodyn.*, **41-44**, 1279-1290.
Theodorsen, T. (1935), "General theory of aerodynamic instability and mechanism of flutter", NACA report No: 496, US Advisory Committee for Aeronautics, Langley, VA.
Tiffany, S. H. and Adams Jr., W. M. (1987), "Nonlinear programming extensions to rational function approximation of unsteady aerodynamics", *Proceedings of AIAA Symp. on Structural Dynamics and Aeroelasticity*, AIAA, Washington, D.C.
Xie, J. and Xiang, H. (1985), "State space method for 3D flutter analysis of bridge structures", *Proc. Asia Pacific Symp on Wind Engineering*, New Delhi, India, 269-276.

CC